We are IntechOpen, the world's leading publisher of Open Access books Built by scientists, for scientists

6,900
Open access books available

185,000
International authors and editors

200M
Downloads

Our authors are among the

154
Countries delivered to

TOP 1%
most cited scientists

12.2%
Contributors from top 500 universities



WEB OF SCIENCE™

Selection of our books indexed in the Book Citation Index in Web of Science™ Core Collection (BKCI)

Interested in publishing with us?
Contact book.department@intechopen.com

Numbers displayed above are based on latest data collected.
For more information visit www.intechopen.com



Chapter

Sedimentation and Proposed Algorithms to Detect the Possible Existence of Vegetation and Humidity in the Landing Area of the Mars Exploration Rover-B (Opportunity)

Emilio Ramírez-Juidías, Katherine Villavicencio-Valero and Arthur Borja

Abstract

Opportunity was launched in 2004 and has been providing interesting data from Mars till 2018. Meridiani Planum was the landing site for the robot. This crater has numerous rock outcrops, which are considered a valuable geological resource that contains keys to the Martian past. In this work, several algorithms have been developed for detecting the possible presence of humidity and vegetation on Mars through the images sent by the Mars Exploration Rover - B Opportunity and by the Viking Orbiter between 1976 and 1980. For this, it was carried out a sedimentary simulation of the study area, as well as an analysis of all the images from the spectral signatures extracted. The results show the existence of three types of water on the surface, as well as concentrations of Neoxanthin, also on landing area surface, that suggest the possible existence of microalgae.

Keywords: humidity, vegetation index, chlorophyll, Meridiani Planum

1. Introduction

In its remote past, Mars exhibited volcanic activity, endured numerous impacts from planetesimals on its surface, but it also possessed an Earth-like atmosphere and surface water. During Mars' formation, some collisions between the planetesimals and the protoplanet ejected material into space. Of the tens of thousands of meteorites found on Earth, about two hundred came from Mars and provide some scientific evidence as to the formation of Mars [1].

Recent discoveries of thousands of exoplanets indicate that planetary systems are the norm rather than the exception in the observable universe. The types of planets that form in a system are dependent on the age of the host star, which is why the older the star, the more likely it is for the planets to contain heavier elements.

It must be emphasized that Mars was formed through an accretion process from volatile-poor planetesimals in the inner solar nebula. The relatively small size of Mars indicates possible Jovian interference during the accretion process. The accretion process and the decay of radioisotopes released gravitational potential energy that melted the Martian protoplanet. Both events led to differentiation into a core–mantle–crust planet structure [2, 3].

It is known from Earth analog studies that most of the tungsten, iron, and other metals sink to the core of a planet in its molten state early in its formation. From radioisotope ratio studies of the Martian meteorites, evidence supports the hypothesis that Mars formed in 2 to 4 million years. However, recent research suggests that tungsten and platinum on the planetesimals themselves could have altered the Martian crust ratios of tungsten, iron, and other metals. The provenance of the two hundred meteorites found on Earth does not provide conclusive evidence of the Martian surface's composition. The latest literature suggests that it is most likely that the small sample of meteorites comes from a few impacts. Those few impacts render the sample size too small to draw accurate conclusions of Martian formation. An alternate hypothesis states that large projectiles with formed cores and mantles bombarded the red planet [4]. According to new modeling, the planetesimals' composition varied enough in ferrophilic element content to provide the tungsten variance, resulting in a heterogeneous Martian mantle. This alternate hypothesis offers an estimate of a Martian formation period of up to 20 Mya [5].

On the other hand, and in relation to the Mars atmosphere, the Mariner mission revealed a fine Martian atmosphere that varies greatly. Because it is thin, the atmosphere of this planet expands rapidly in the warmer months and contracts rapidly in the colder months [6]. In general, it can be said that the atmosphere of the red planet is similar in composition to that of Venus but much thinner. Carbon dioxide comprises about 95% of the atmosphere, with the rest being nitrogen (3%) and argon (1%). The carbon dioxide freezes over the poles, and frozen water lays underneath the frozen carbon dioxide layer.

Regarding the geology of Mars, it is interesting to comment that this planet has two vastly different hemispheres (**Figure 1**), that is, the older heavily cratered highlands of the Southern Hemisphere and the Northern Hemisphere's younger lowland plains. Mars presents extreme topography when compared to Earth and even the Moon. A marked 30-kilometer elevation difference exists between the summit of Olympus Mons and the floor of the Hellas Basin. The hemispheres' difference can be explained by possible volcanic eruptions or seas that smoothed out the Northern Hemisphere. In addition to the highland terrains and the lowland

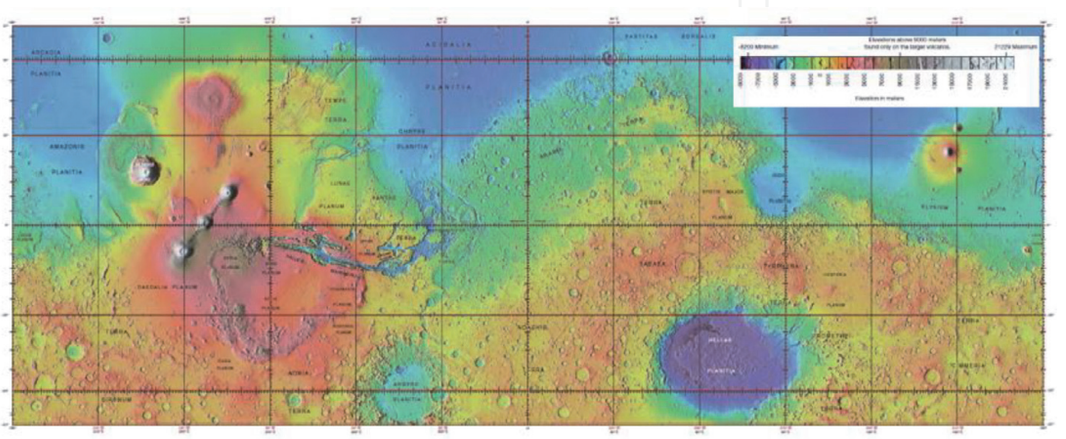


Figure 1.
MOLA global image of Mars surface [7].

plains, Mars features other landscapes that include the polar terrains, the Tharsis and Elysium volcanic terrains, and chaotic terrains.

According to [4, 5], Mars also features numerous buried impact basins dating from its early history. Other geologic features visible on the surface include dendritic runoff channels. These features display river-like patterns that evidence precipitation or snowmelt runoff flow. In the equatorial regions, outflow channels evidence cataclysmic events of the release of underground ice melt.

For the present work, and although studying Martian rocks and mineral geochemistry provides essential clues as to the conditions when they formed, it must be taken into account that it is well understood from the study of Earth analogs that chemical systems tend toward equilibrium reactions that yield the lowest energy and, therefore, the most chemically stable compounds within specific environments. As a consequence of this, it is interesting to mention that chemical weathering and erosion of basaltic and other igneous rocks produce distinct sediments and minerals that provide a detailed history in terms of temperature, pressure, pH, atmospheric composition, etc., that led to the formation of specific minerals.

Although numerous studies of various nature have been carried out on Mars to date, none of them have studied in depth the phenomena of water erosion that occur on the surface of Mars. In the same way, no scientific work has used state-of-the-art remote sensing techniques, based on machine learning, to be able to obtain algorithms capable of predicting both surface moisture content and indications of the presence of some type of photosynthetic organism. It is therefore that this chapter is innovative, in addition to pretending to be a reference in the bibliography about similar studies on rocky planets and moons in our solar system.

2. Study area

As is known, Opportunity (Mars Exploration Rover-B) landed in the Eagle crater, located in the Meridiani Planum (0,2° N; 357,5° E in planetocentric coordinates), on January 25, 2004.

The reason why Opportunity was sent to Meridiani Planum was because the Thermal Emission Spectrometer (TES), of the Mars Global Surveyor mission, found, from its orbit, crystalline gray hematite on the surface of Mars in an amount around 20%. Hematite is an iron oxide that, usually its gray crystalline variety, is formed in association with liquid water on Earth.

According to [8], at Opportunity's landing site, gray hematite within a kind of spherules was found in outcrops of soft and stratified sandstone rocks. It should be emphasized that for these structures to form, the acidic aqueous alteration of basalt rocks rich in goethite (a mineral that contains iron) was necessary. Subsequently, the alteration of the goethite gave rise to hematite, which formed spherules in the rocks and, as these were worn away by the action of acidic water, they accumulated on the surface.

In relation to what was previously specified, and based on [9, 10], it is interesting to say that the soil of Meridiani Planum is composed of fine grains of basalt sand, in addition to a surface of spherules, with a high content of hematite, and other granules. According to [9], the erosion by action of the wind is visible, as well as small impacts of craters and layers of sedimentary rocks, finely laminated, rich in sulfides [10] and sulphated salts. Regarding cross lamination, it is known that on small scales it provides evidence that liquid water flowed through the study area. These rocks were probably a mixture of siliciclastic and chemical sediments formed in an episode of shallow water flooding followed by evaporation, exposure, and settling, similar to what occurs in a salt-marsh on Earth [11].

3. Material and methods

For this study, a total of 49 control points were selected, using planetocentric coordinates (**Table 1**), in the study area (**Figure 2**) based on the coverage of images downloaded from the Pilot tool [12], and captured by the Viking Orbiter between 1976 and 1980. The purpose, of using images from the Viking Orbiter, is none other than to check whether water and chlorophyll pigment-producing organisms existed on the surface of Mars in that period.

In total, 942 images were obtained, all in the planetocentric coordinate system, and whose geographic coordinates, which make up the area from which the control points have been established, have values, relative to the upper left corner of the study area, of 10° latitude and − 15° longitude, while those corresponding to the lower right corner are −10° latitude and 15° longitude.

In order to eliminate the possible atmospheric effects present in the information of each pixel of the downloaded images, the procedure patented by the main author of this work was used [13]. This procedure uses RGB coded bands

Control point n°	Latitude (°)	Longitude (°)	Control point n°	Latitude (°)	Longitude (°)
1	10	−15	**26**	0	5
2	10	−10	**27**	0	10
3	10	−5	**28**	0	15
4	10	0	**29**	−3	−15
5	10	5	**30**	−3	−10
6	10	10	**31**	−3	−5
7	10	15	**32**	−3	0
8	7	−15	**33**	−3	5
9	7	−10	**34**	−3	10
10	7	−5	**35**	−3	15
11	7	0	**36**	−7	−15
12	7	5	**37**	−7	−10
13	7	10	**38**	−7	−5
14	7	15	**39**	−7	0
15	3	−15	**40**	−7	5
16	3	−10	**41**	−7	10
17	3	−5	**42**	−7	15
18	3	0	**43**	−10	−15
19	3	5	**44**	−10	−10
20	3	10	**45**	−10	−5
21	3	15	**46**	−10	0
22	0	−15	**47**	−10	5
23	0	−10	**48**	−10	10
24	0	−5	**49**	−10	15
25	0	0			

Table 1.
Control points on Mars surface where spectral signature has been obtained.

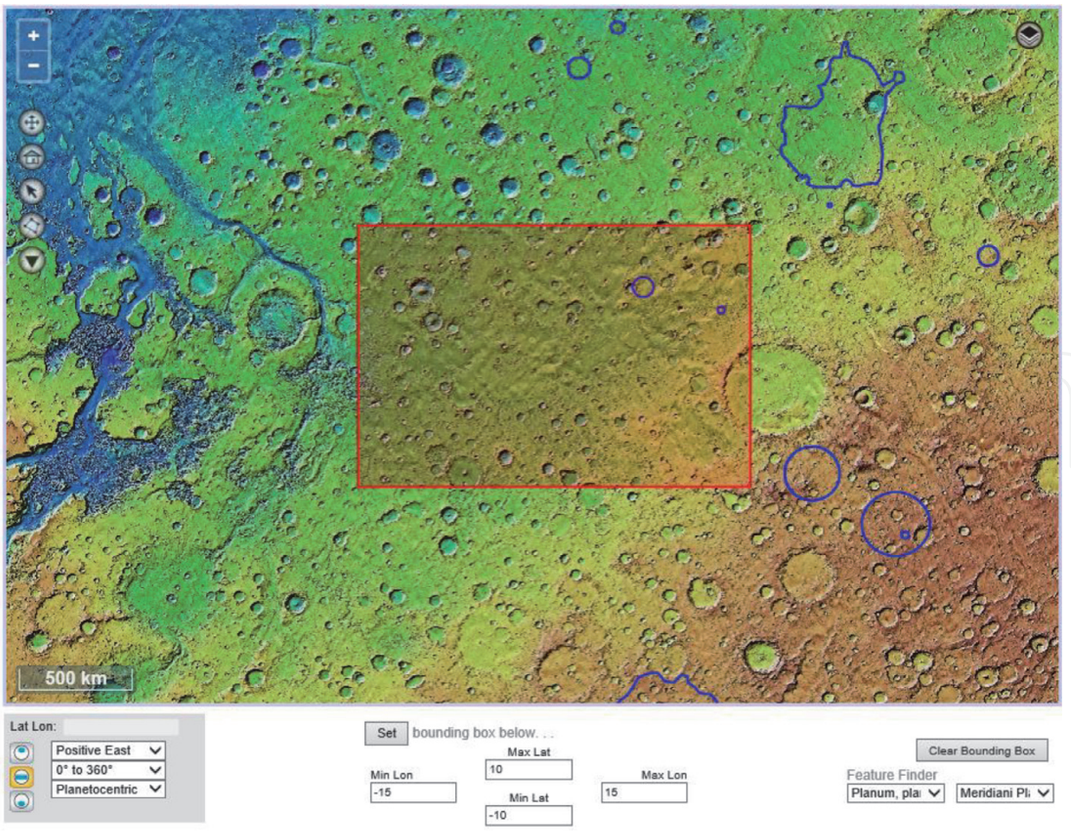


Figure 2.
Location of the study area.

(Red-Green-Red), which have a similar effect to that obtained when a satellite image is corrected for bias and field. The resulting images will be displayed in three colors (magenta, green and dark green), the latter being the one shown in those areas whose relative moisture content is high compared to the rest of areas of same image. It should be emphasized that the coding of visible bands, by means of the patented procedure obtained by [13], results in a series of spectral bands that provide more information than those corresponding only to the visible spectrum, since it allows to extract, from each pixel, the information found in the region from ultraviolet to near infrared.

In order to find algorithms capable of detecting both the moisture content and the existence of chlorophyll pigment-producing organisms on Mars surface, the spectral signatures of the 49 control points specified above have been obtained, each of which was compared with the spectral signatures encoded (with range of wavelengths in nm) of different types of water, as well as different types of ice, existing in certain areas of the Earth (**Table 2**), which are presented in **Figures 3** and **4**.

In the same way, a massive search for plant pigments was carried out at the pixel level, using the Plant Pigment Ratio (PPR) [14], to later relate it to the Coded Normalized Vegetation Index (CNDVI) obtained by [13]. Equations of the PPR and CNDVI indices are shown in Eqs. (1) and (2) respectively.

$$PPR\left(mol \cdot mol^{-1} of\ Clhorophill\right) = \frac{(Blue - Green)}{(Blue + Green)} \tag{1}$$

$$CNDVI = \frac{(Red\ cod - Green\ cod)}{(Red\ cod + Green\ cod)}\ \left(r = 0,85; R^2 = 0,91\right) \tag{2}$$

In another vein, a simulation of the transported soil was carried out, as a consequence of erosive processes, in the study area. To carry out this analysis, a total of 82

Water type 1	Mean spectral signature of water on Earth
Freshwater	Mean spectral signature of freshwater on Earth
Saltwater	Mean spectral signature of saltwater on Earth
Acid water 1	Mean spectral signature of the acidic water belonging to the South Minas de Riotinto reservoir (Huelva, Spain)
Acid water 2	Mean spectral signature of the acidic water belonging to the North Minas de Riotinto reservoir (Huelva, Spain)
Turbid water	Mean spectral signature of turbid water existing in the Guadalquivir River (South of the Iberian Peninsula, Spain)
Frozen water (type 1)	Mean spectral signature of water ice on Earth
Frozen water (type 2)	Mean spectral signature of the Sierra Nevada water ice (Granada, Spain)

Table 2.
Different types of both water and ice, existing in the Earth, taken as reference.

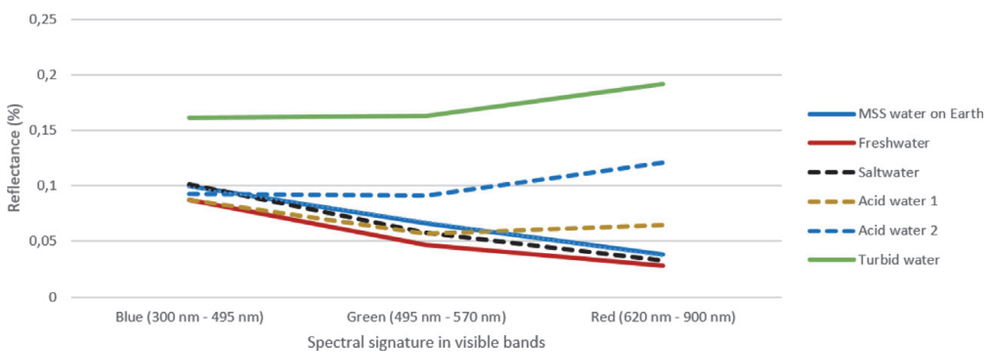


Figure 3.
Spectral signatures of different types of water in the visible spectrum (MSS water on Earth is the Mean Spectral Signature of water on Earth).

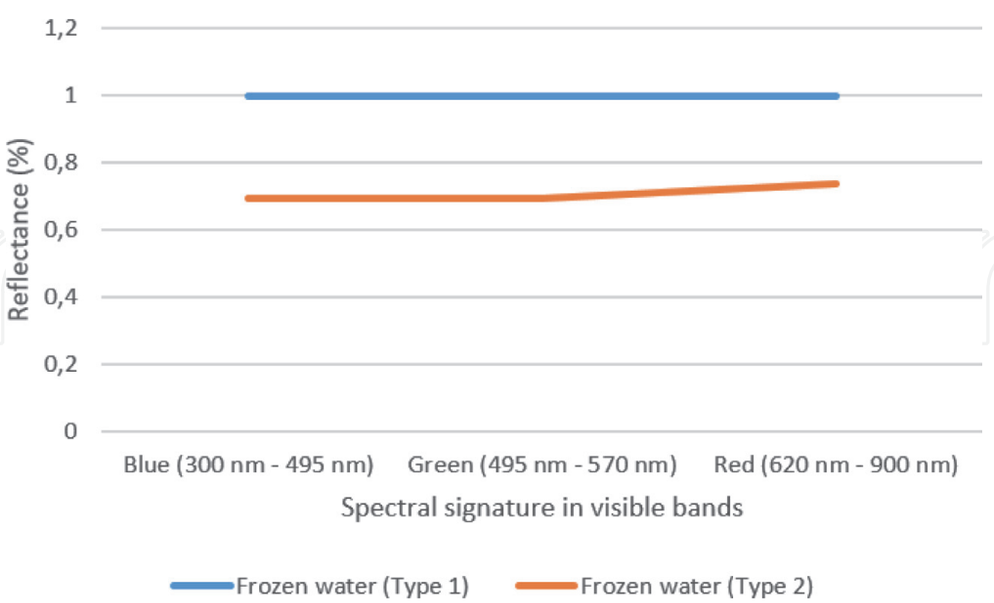


Figure 4.
Spectral signatures of two types of frozen water in the visible spectrum.

control points were established, in the form of a rectangular mesh, in the study area, although taking the area covered by Opportunity as a reference.

As a consequence of not having initial topographic values of the soil of Mars, nor of how they have varied over time, the total transported soil is calculated using the

equation proposed by [11] for salt-marshes. It must be taken into account that the small diameter of the pebbles existing in the study area, which have been measured from the images captured by Opportunity using ImageJ software, are similar to the diameter of those existing in salt-marshes on Earth with a very slow water course velocity (such as that existing at Tinto or Odiel salt-marshes, or even at both Isla Cristina or Doñana salt-marshes). Therefore, the model used is shown in Eq. (3):

$$y = 0,032 - 0,133 \cdot SD - 1,164 \cdot T \ \left(r = 0,973; R^2 = 0,941\right) \tag{3}$$

Where "y" is the prediction of volume of eroded soil in hm^3, "SD" is the equivalent area (km^2) where the eroded volume has occurred, and "T" is the height counted from the lowest level of the bed depth, in each control point, in study area (positive values represent sediment deposition, while negative values represent soil erosion).

In order to be able to calculate, with sufficient precision and through iterative processes [13], the volume of eroded soil, the Digital Terrain Model (DTM) of the Mars Orbiter Laser Altimeter (MOLA) has been used.

In relation to the above, a model was obtained, from which, to calculate the water flow velocity that existed in Meridiani Planum based on the pebbles diameter found in the Opportunity images. This model was compared with the one obtained by the second and third author of this chapter in a zone of slow water flow velocity of the Chaqui river in Bucay (Ecuador) and in a stream located in Bonita Creek (CA, USA) respectively.

4. Results and discussion

4.1 Analysis of spectral signatures

After comparing the spectral signatures of each of the 49 control points (**Table 1**) established in the study area, with the spectral signatures encoded (with range of wavelengths in nm) of the Earth (**Figures 3** and **4**), coincidences have been found in three of them (**Figure 5**), and more specifically with those corresponding to acid water 2, turbid water and frozen water (type 2), although only in 39 control points (**Table 3**).

On the other hand, and as a consequence of the existence of perchlorate salt (it enables the existence of acid water, in addition to facilitating the water evaporation at temperatures below 0°C) on Mars surface [15], a new algorithm, called Moisture Soil Index on Mars (MSIM), has been obtained, with which it is possible to obtain the humidity percentage in Martian soil. The expression of the MSIM is shown in Eq. (4):

$$MSIM\ (\%) = 10 \cdot \left[1 - \left(\frac{Blue\ band}{Red\ band}\right)^{1,5}\right] \ \left(r = 0,71; R^2 = 0,735\right) \tag{4}$$

After comparing the MSIM with the WEH moisture index (it corresponds to the amount of hydrogen molecules in the water) established by [16] (**Figure 6**) it is observed that, although there is no relationship between both indices, it is true that a high WEH corresponds to high MSIM and vice versa.

In order to facilitate the use of this new index, an estimate of it can be obtained from the planetocentric coordinates of Mars, as shown in Eq. (5).

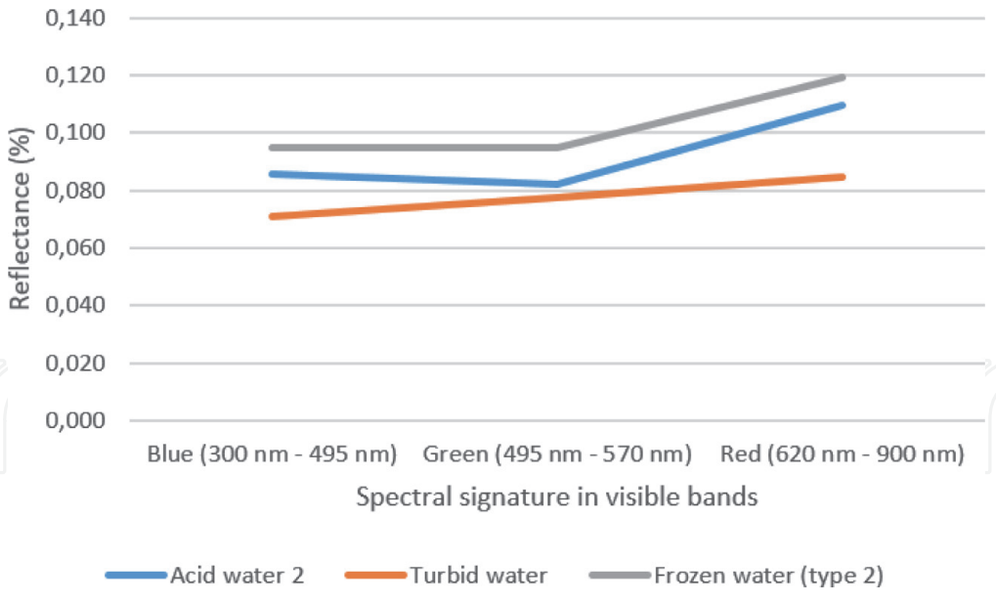


Figure 5.
Spectral signatures found on Mars.

	Acid water 2						Turbid water		Frozen water (type 2)		
C.P.	**Lat**	**Long**	**C.P.**	**Lat**	**Long**	**C.P.**	**Lat**	**Long**	**C.P.**	**Lat**	**Long**
1	10°	−15°	**17**	3°	−5°	**11**	7°	0°	**18**	3°	0°
2	10°	−10°	**21**	3°	15°	**19**	3°	5°			
3	10°	−5°	**23**	0°	−10°	**20**	3°	10°			
4	10°	0°	**24**	0°	−5°	**22**	0°	−15°			
5	10°	5°	**27**	0°	10°	**26**	0°	5°			
6	10°	10°	**28**	0°	15°	**31**	−3°	−5°			
7	10°	15°	**29**	−3°	−15°	**36**	−7°	−15°			
8	7°	−15°	**30**	−3°	−10°	**41**	−7°	10°			
9	7°	−10°	**34**	−3°	10°	**43**	−10°	−15°			
10	7°	−5°	**35**	−3°	15°	**44**	−10°	−10°			
13	7°	10°	**37**	−7°	−10°	**47**	−10°	5°			
14	7°	15°	**45**	−10°	−5°						
15	3°	−15°	**49**	−10	15°						
16	3°	−10°									

Table 3.
Planetocentric coordinates of Mars with coincidences in spectral signature with Earth (C.P. = Control Point).

$$MSIM\ (\%) = -0,32 + 0,014 \cdot L + 0,063 \cdot Lat - 0,033 \cdot Lon \ \left(r = 0,71; R^2 = 0,47\right) \tag{5}$$

Knowing that:

L = Luminance of each pixel = Red + Green + (Blue/3). It is a dimensionless index.

Lat = Latitude in decimal degrees.

Lon = Longitude in decimal degrees.

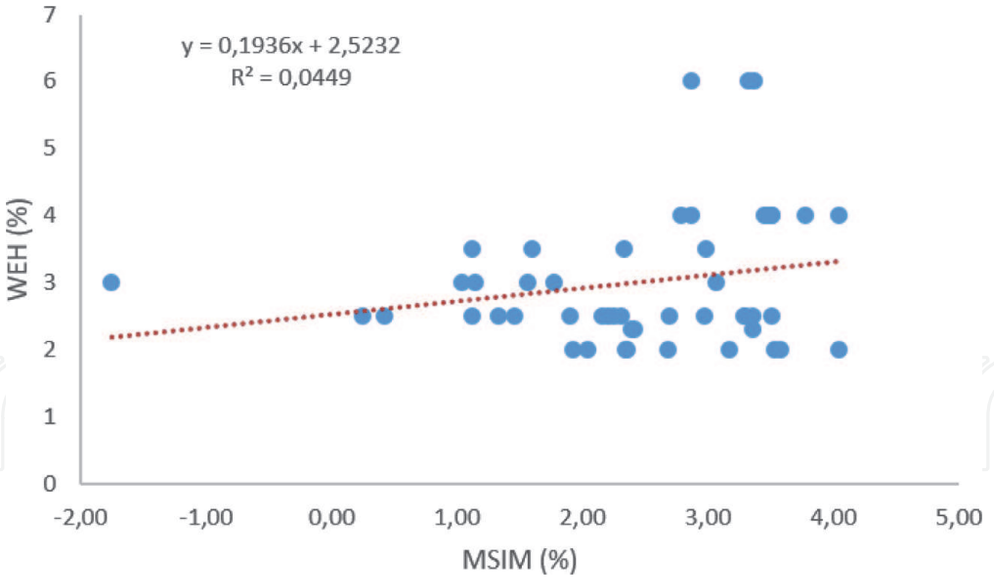


Figure 6.
Comparison between WEH [16] and MSIM obtained for Mars in the study area.

4.2 Analysis of moisture sources from Opportunity images

As is well known, according to [17], soil moisture plays a fundamental role both in the hydrological cycle and in land-atmosphere interactions. However, there are several studies in which the importance of the soil has been analyzed in various scientific areas, such as in climate simulations and meteorological prediction [18], in precipitation and runoff models [19] or in evapotranspiration [20] among others.

In this sense, and with regard to Eagle Crater, [21] specified that the outcrop, shown in the upper part of **Figure 7**, was wet by salt water, in addition to containing high concentrations of hematite and jarosite, minerals that form from the alteration of rocks in the presence of acidic water.

At this point, it is very important to mention that, according to [23], depending on the texture and structure of the soils, these can contain a certain amount of moisture that is normally generated as a result of a rainfall event [24], that saturates the soil causing a portion to drain towards the interior due to the gravity force.

Regarding the Endurance crater, Opportunity made a total of seven holes using the rock abrasion tool. Likewise, the rover made combined mosaic images like the one shown in **Figure 8** on the left. Evidence of fine-grained red hematite was observed around the drill area [21].

It is convenient to emphasize that the dark green area, selected with the red arrow in **Figure 8** right, contains iron oxide compounds, which, on the surface of Mars, have a color similar to that of hematite on Earth (gray).

In another vein, according to [26], the studied area by Opportunity have sandstones rich in sulfates, which indicates the existence of past erosion by the action of both the wind and by a slow water flow as a result of the possible formation of ephemeral (and shallow) lakes.

In **Figure 9** right it can be seen that the dark green coloration, which indicates the presence of moisture [13], is found in the predominant stratum on the right. This stratum is formed by a lumpy rock called Wopmay located on the inner of Endurance slopes. It is believed that this type of rock is the consequence of an alteration due to the presence of water [27].

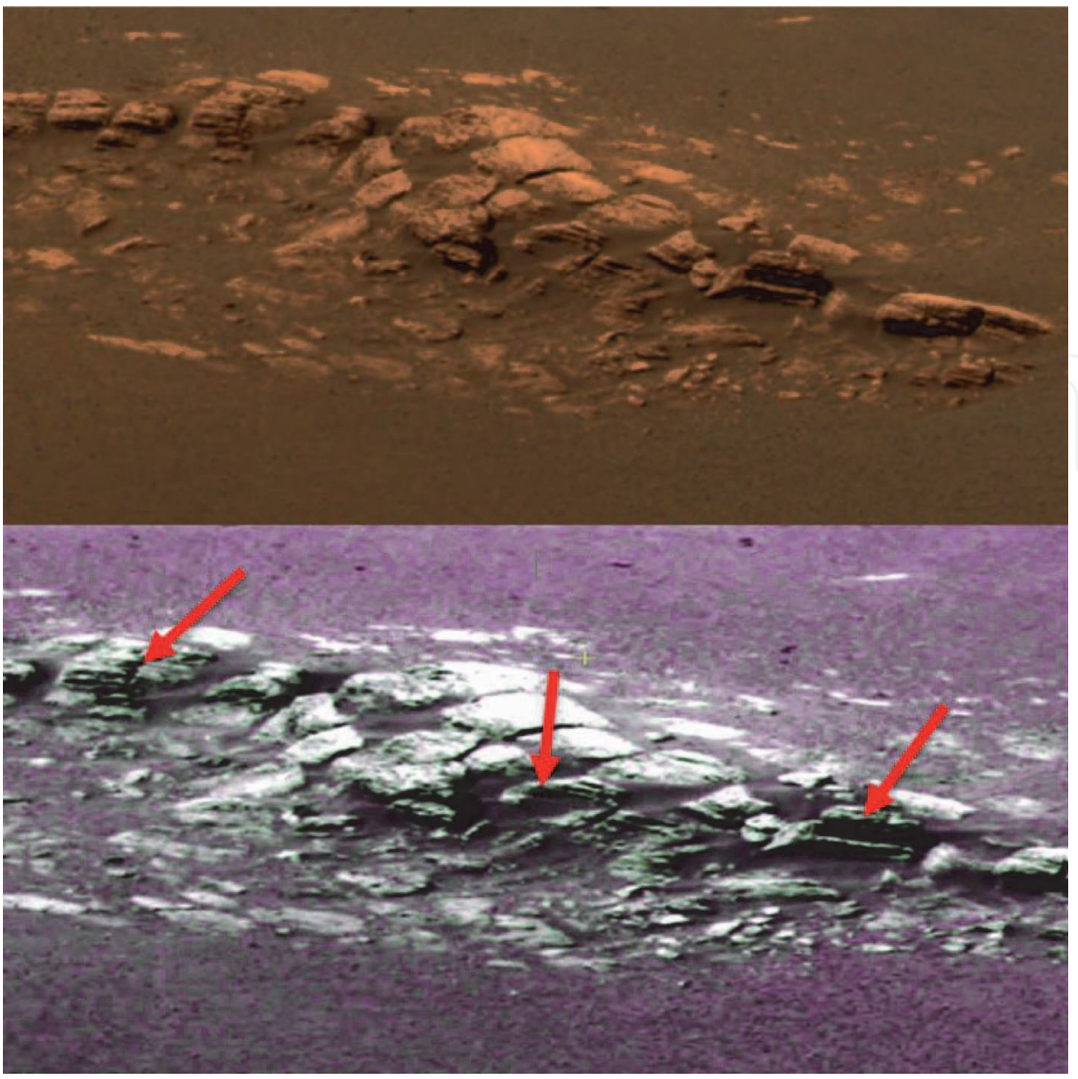


Figure 7.
Image taken by Opportunity (Sol 4) at Eagle Crater [22]. The lower image shows the wet areas (red arrows) after subjecting the upper image to the process patented by [13].

4.3 Model to obtain water flow velocity based on pebbles diameter

To obtain this model, both in the Chaqui River (Bucay, Ecuador) and in a stream located in Bonita Creek (California, USA), the water velocity was calculated at a series of points established in field (15 in Ecuador and 10 in the USA), to later measure the average pebbles diameter at those same points. Subsequently, with the use of genetically modified algorithms, although taking into account the gravity of Mars (3,7 m/s^2), the water flow velocity that should exist on Mars was calculated to have pebbles of the same diameter as those measured in the specified sampling points. For this process, the DTM obtained by MOLA was also used. The result was that the water flow velocity on Mars having to be in a relationship as shown in Eq. (6):

$$V_{on\ Mars} = \frac{e^{D_{on\ Earth}}}{3} \quad (r = 0,91; R^2 = 0,99) \tag{6}$$

Once the water velocity on Mars was obtained, it was represented against the diameter, obtaining the model presented in **Figure 10**, and from which it is possible to calculate the water velocity in any area of Mars as long as there is evidence that it was covered by water. In Eq. (7) the model presented in **Figure 10** is appropriately specified.

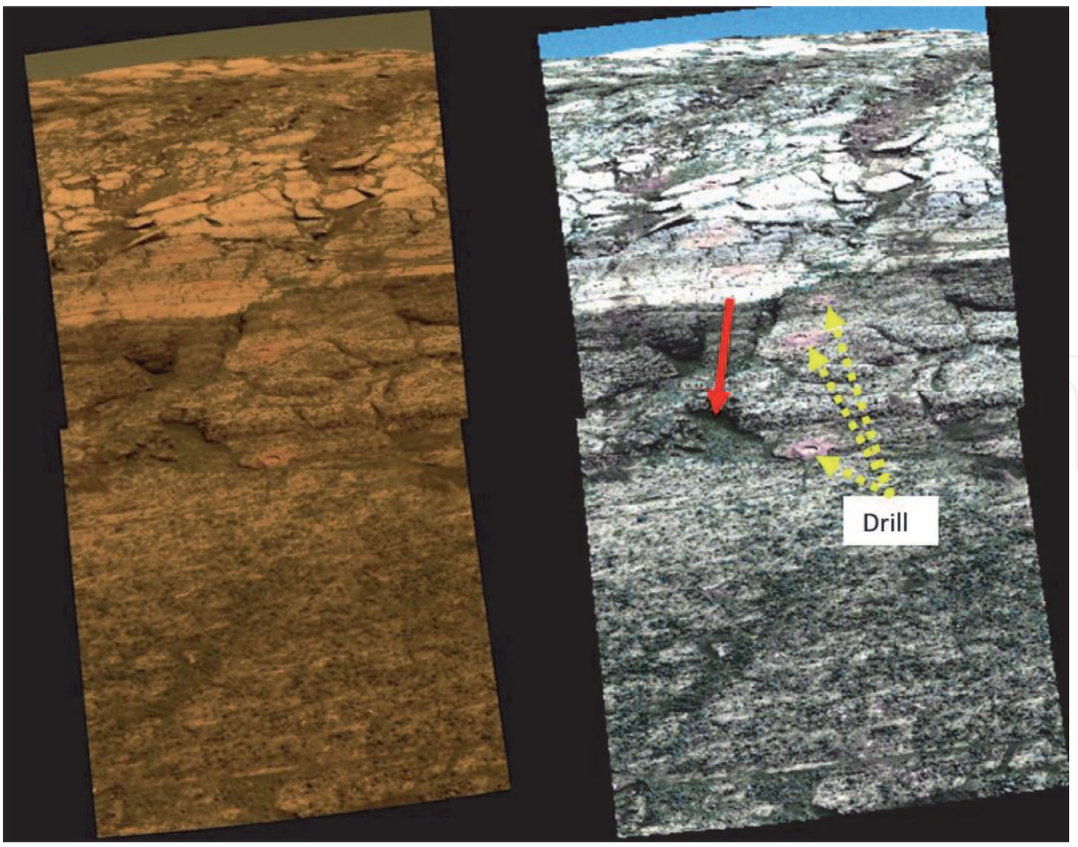


Figure 8.
Image taken by Opportunity (Sol 173) at Endurance Crater [25]. The right image shows the wet areas (red arrow) after subjecting the upper image to the process patented by [13].

$$V_{on\ Mars} = 0,4961 \cdot D_{pebbles\ on\ Mars} + 0,3025 \left(r = 0,98; R^2 = 0,99\right) \qquad (7)$$

Authors want to record that the model shown in Eq. (7) has been used by two studies, pending publication, in the areas of the Spirit and Curiosity rovers respectively, obtaining results that are fully consistent with the reality of Mars.

Later, with the use of the free software ImageJ (**Figure 11**), the pebbles diameter in the study area was measured. In **Figure 11** is shown a measure that no corresponding to a pebbles only to show, clearly, the procedure used. Pebbles diameters measured in study area fit perfectly (see **Figure 10**) with Eq. (7).

4.4 Prediction of erosion in Meridiani Planum

As can be seen in **Figure 10**, as well as in Eq. (7), the water velocities obtained on Mars are in the same velocities range as those obtained in a salt-marsh, for this reason the model shown in Eq. (3) and proposed by [11] has been used.

The transport of sediments in study area has been calculated through an evaluation to pixel level (**Figure 12**) using the DTM obtained by MOLA and the patented procedure by [13]. In this figure, sediment transport is simulated based on climatic conditions [28] on Mars and a surface shape factor dependent of algorithm used by [13].

Throughout its history, and according to [24], the surface of Mars has had a very active hydrological cycle, which has given rise to a network of valleys formed, mainly, by the surface flow erosion, leaving, as secondary factor, erosion due to groundwater seepage. It is precisely this fact that makes it possible for the depth profile at the control points 12, 15 and 77 to reach the values −1437,47 m, −1676,72 m and − 2873,03 m respectively.

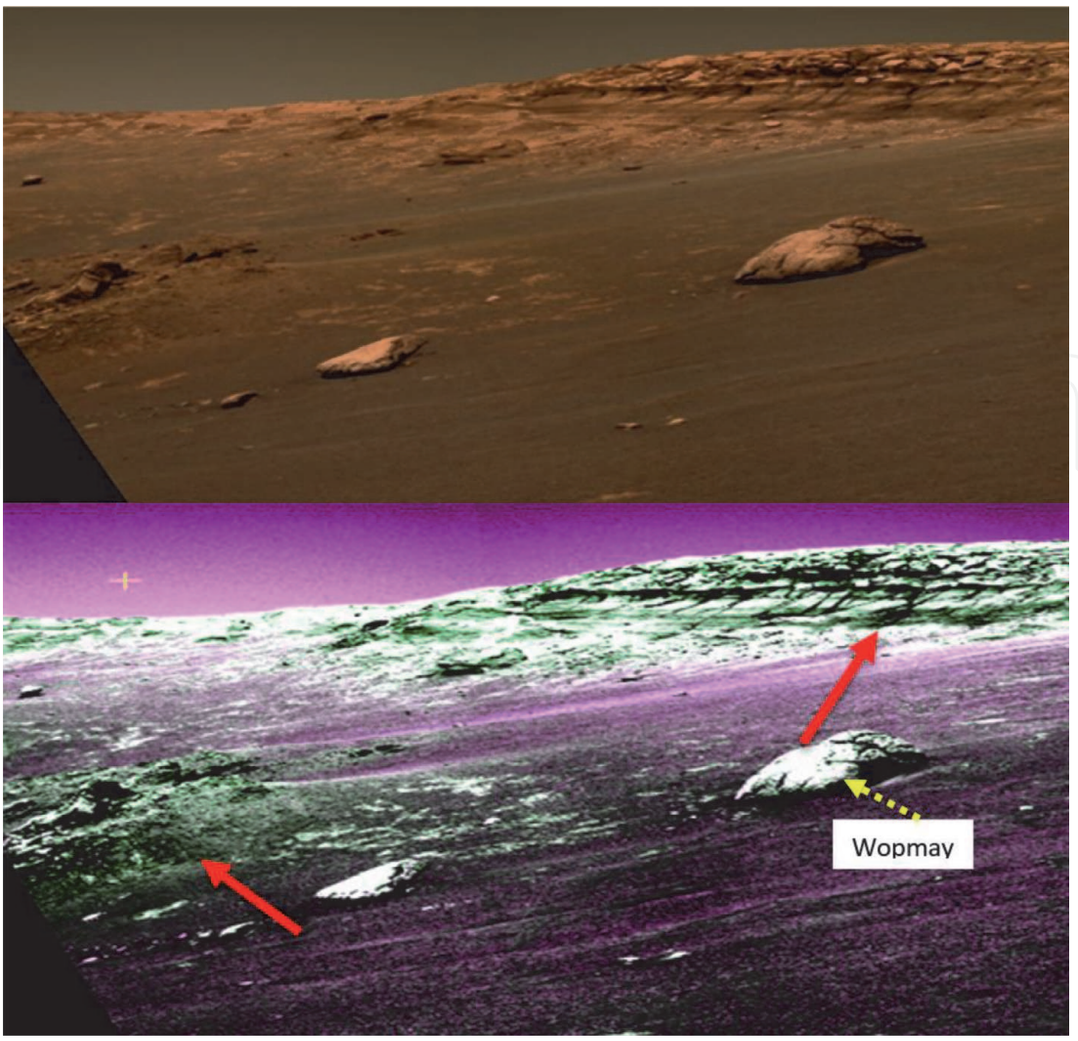


Figure 9.
Image taken by Opportunity (Sol 248) at Endurance Crater [27]. The right image shows the wet areas (red arrows) after subjecting the upper image to the process patented by [13].

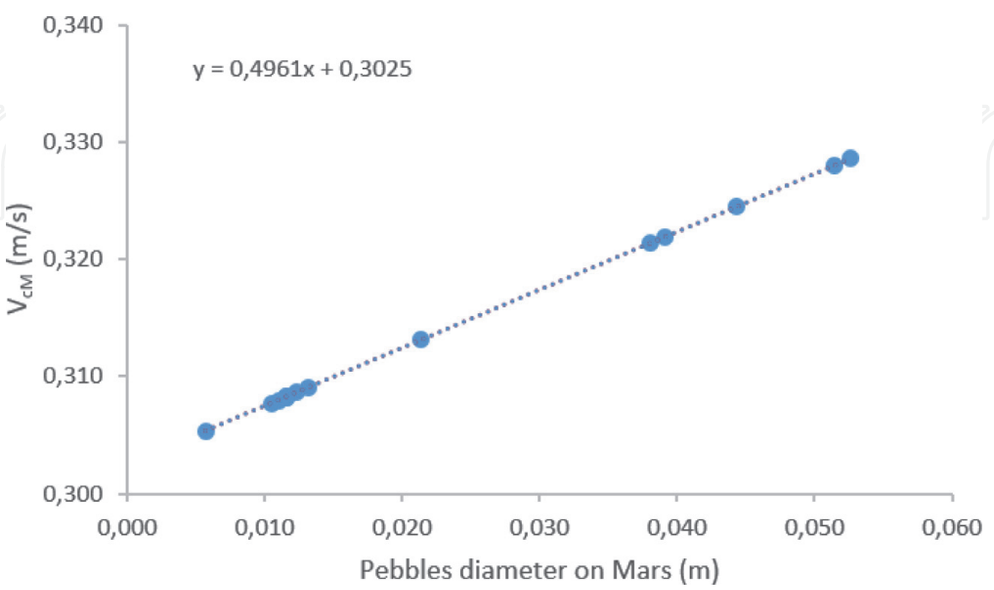


Figure 10.
Relationship between the water velocity (m/s) and the pebbles diameter (m) on Mars surface.

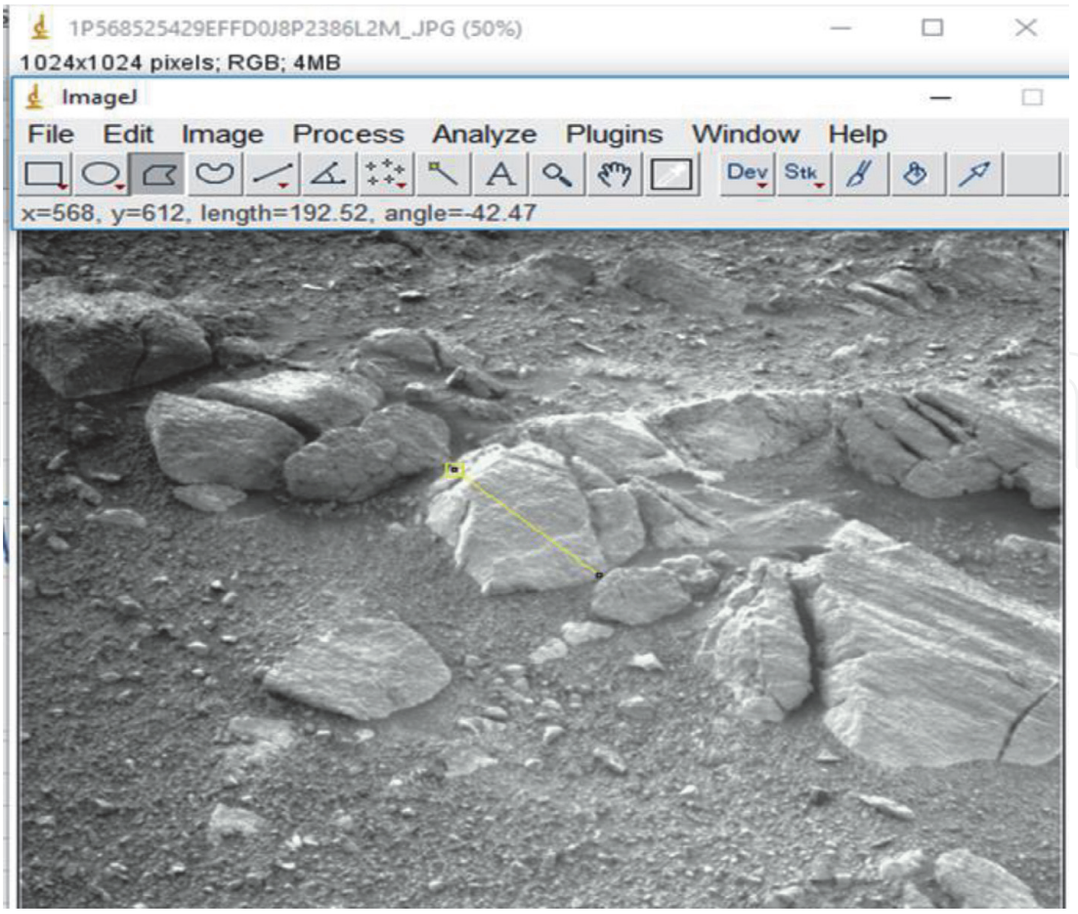


Figure 11.
Procedure used to measure diameter (length measurements are in pixels).

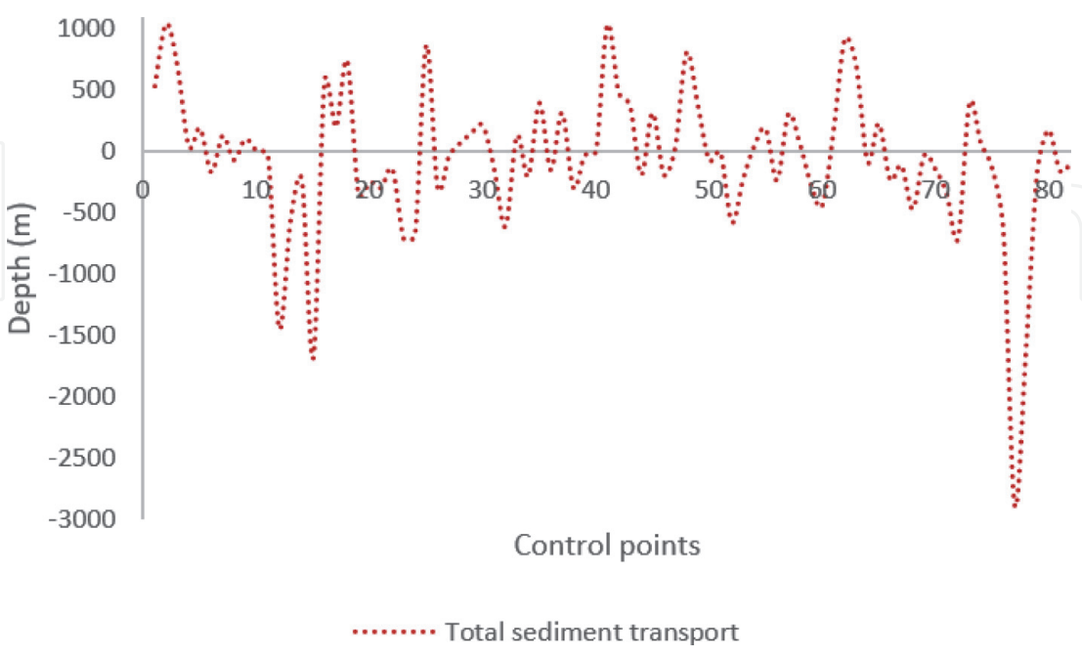


Figure 12.
Variation of the depth in terms of sediment transport in study area (positive values = soil deposition; negative values = soil erosion).

4.5 Possible existence of chlorophyll pigment-producing organisms on Mars surface

After the analysis carried out at the pixel level, in order to find some trace of vegetal life, it has been obtained that the PPR index [14] has varied between −0,10 and 0,09 mol · mol^{-1} of chlorophyll (**Figure 13**). It must be specified that on Earth, values between 0 and 0,1 mol · mol^{-1} chlorophyll (both inclusive) correspond to Neoxanthin.

According to [29], Neoxanthin is a type of carotenoid and xanthophyll existing in some types of plants, and whose function is to protect the plant against photo-oxidative stress.

It must be taken into account that, on Earth, the production of Neoxanthin by vegetables remains constant at temperatures of up to −20°C, easily achievable on Mars, while the production of Carotenoids and Beta-Carotenoids decreases at temperatures below 0°C. For this reason, there is a certain probability that organisms that synthesize, mainly, Neoxanthin may exist on Mars surface.

After the bibliographic review carried out, and according to [30], one of the organisms that synthesizes Neoxanthin, and that may possibly be present on the Mars surface, are microalgae with a protected cell wall. These organisms can survive in extreme conditions as long as they are adapted to the environment.

It is known that microalgae proliferate on Earth in conditions of contamination of the aqueous environment, which can be found on Mars due to the existence of perchlorate salt. In the same way, and after the analysis of the spectral signatures, acidic water and turbid water have been found, so the existence of microalgae is reinforced.

Given the possible existence of microalgae on Mars, the new CNDVI (Eq. (2)) was obtained, whose relationship with the PPR index is presented in **Figure 14**. As can be seen in **Figure 14**, relationship between both variables is quite good, so the idea of the possible existence of microalgae, or Neoxanthin-producing organisms, on Mars becomes more consistent.

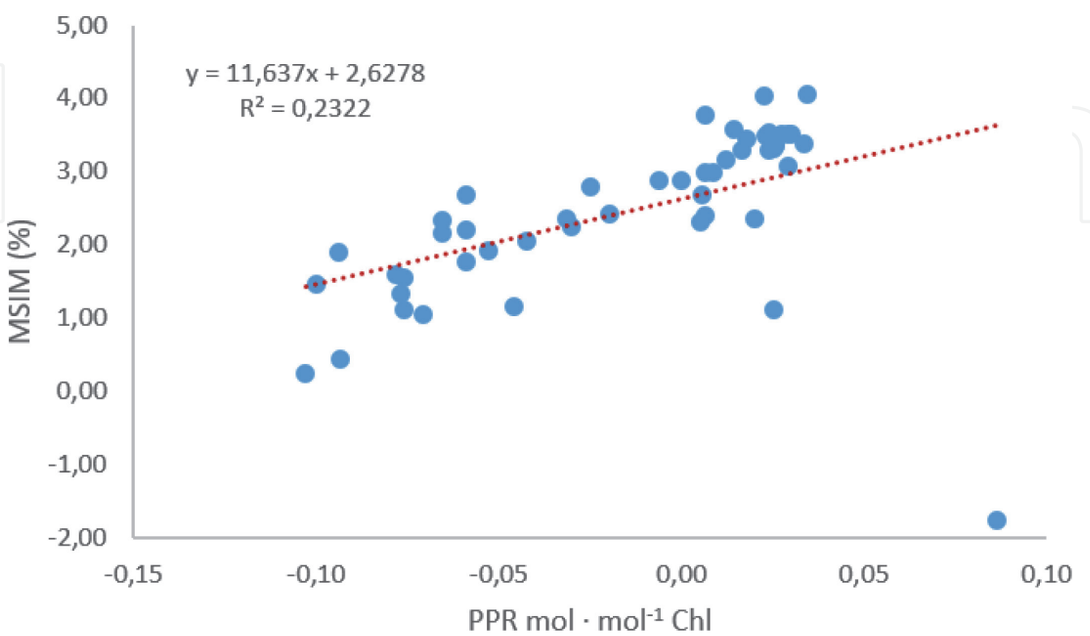


Figure 13.
Relationship between the MSIM and the PPR index in study area.

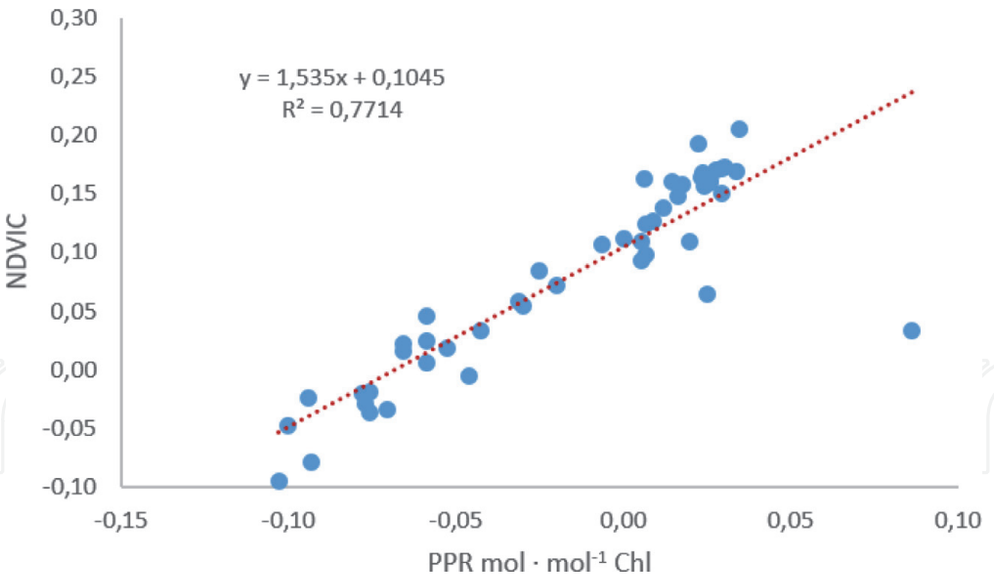


Figure 14.
Relationship between the CNDVI and the PPR index in study area.

5. Conclusions

In this study, different novel aspects related to Meridiani Planum, as well as Opportunity, have been shown.

Logically, despite the fact that the results obtained are encouraging in many aspects, other hypotheses must be taken into account in order to complement not only this research work, but also all those that are carried out from this study.

However, we must pay attention to the well-known seasonal process of water mobility on Mars as a result of perchlorate salts, since a phenomenon similar to FVAT [31] can exist, due to which the transit of water and salt of perchlorate towards the surface is possible from certain environmental conditions of relative humidity, pressure, temperature, as well as a determined concentration level of perchlorate salt in the water, be it acidic or turbid.

During the present work, the presence of aqueous minerals has been corroborated, although it is true that the samples collected by Opportunity, as well as other rovers that are in operation on Mars, have sufficient reliability. In this regard, this study shows that the data obtained (from the 942 images analyzed) by the Viking Orbiter have the same reliability, especially as a result of the fact that they have made it possible to corroborate aspects, phenomena and situations that occurred on Mars, and that Opportunity, Spirit and Curiosity had demonstrated. A special mention should be made of Perseverance, whose data will allow us to advance our knowledge of the red planet.

Authors want to highlight, given that they have carried out the same study in the areas covered by Spirit and Curiosity, that the results obtained are similar, although in the area covered by Curiosity there is evidence of a lower amount of PPR. On the other hand, in the Gusev crater, area where Spirit is located, a spectral signature corresponding to saltwater has been found.

Finally, it must be emphasized the importance of new technologies, patented processes, as well as the development of new advanced calculation tools capable of jointly simulating all possible situations that may occur on any rocky planet or moon existing, since in this way the advancement of knowledge in those worlds will be more efficient.

Conflict of interest

Authors declare no conflict of interest.

IntechOpen

Author details

Emilio Ramírez-Juidías[1*], Katherine Villavicencio-Valero[2] and Arthur Borja[3]

1 University of Seville, Seville, Spain

2 International Research School of Planetary Sciences (U.G. D'Annunzio), Pescara, Italy

3 Bayer School, USA

*Address all correspondence to: erjuidias@us.es

IntechOpen

© 2021 The Author(s). Licensee IntechOpen. This chapter is distributed under the terms of the Creative Commons Attribution License (http://creativecommons.org/licenses/by/3.0), which permits unrestricted use, distribution, and reproduction in any medium, provided the original work is properly cited. CC BY

References

[1] Greenwood RC, Burbine TH, Franchi IA. Linking asteroids and meteorites to the primordial planetesimal population. Geochimica et Cosmochimica Acta. 2020;277: 377-406. DOI: 10.1016/j.gca.2020.02.004

[2] Gaffey MJ. The early solar system. In: Whittet DCB, editors. Planetary and Interstellar Processes Relevant to the Origins of Life. Springer, Dordrecht; 1997. p. 185-203. DOI: 10.1007/978-94-015-8907-9_10

[3] Rauchfuss H, Mitchell TN. The cosmos, the solar system and the primeval Earth. In: Chemical Evolution and the Origin of Life. Springer, Berlin, Heidelberg; 2009. p. 17-41. DOI: 10.1007/978-3-540-78823-2_2

[4] Manske L, Marchi S, Plesa AC, Wünnemann K. Impact melting upon basin formation on early Mars. Icarus. 2021;357:1-13. DOI: 10.1016/j.icarus.2020.114128

[5] Marchi S, Walker RJ, Canup RM. A compositionally heterogeneous Martian mantle due to late accretion. Science Advances. 2020;6:1-7. DOI: 10.1126/sciadv.aay2338

[6] Catling DC, Zahnle KJ. The planetary air leak. Scientific American. 2009;300 (5):36-43. DOI: http://www.jstor.org/stable/26001341

[7] USGS. Planetary names [Internet]. 2021. Available from: https://planetarynames.wr.usgs.gov/images/mola_regional.pdf [Accessed: 2021-02-05]

[8] NASA/JPL-Caltech/Arizona State University. Mars exploration program: Meridiani planum [Internet]. 2012. Available from: https://mars.nasa.gov/resources/5260/meridiani-planum/ [Accessed: 2021-02-05]

[9] Hynek BM, Di Achille G. Geologic map of Meridiani Planum, Mars. US Geological Survey Scientific Investigations Map [Internet]. 2017; 3356:1-13. Available from: http://citeseerx.ist.psu.edu/viewdoc/download?doi=10.1.1.1071.8324&rep=rep1&type=pdf [Accessed: 2021-02-05]

[10] McCollom M, Hynek B. Geochemical data indicate highly similar sediment compositions for the Grasberg and Burns formations on Meridiani Planum, Mars. Earth and Planetary Science Letters. 2021;557:1-13. DOI: 10.1016/j.epsl.2020.116729

[11] Ramírez-Juidías E, Víquez-Urraco F, Noguero-Hernández D. Sedimentary processes in the Isla Cristina salt-marshes: geomorphological changes of landscape. Ocean & Coastal Management. 2017;143:148-153. DOI: 10.1016/j.ocecoaman.2016.11.007

[12] USGS, NASA. Planetary Image Locator Tool [Internet]. 2008. Available from: https://pilot.wr.usgs.gov/ [Accessed: 2021-01-10]

[13] Ramírez-Juidías E, Pozo-Morales L, Galán-Ortiz L. Procedure for ontaining a remote sensed image from a photograph. Patent n° ES2537783B2 (2015-09-29 publication of the patent concession). International Patent n° WO2014198974A1. Universidad de Sevilla. 2015. Available from: http://consultas2.oepm.es/InvenesWeb/detalle?referencia=P201300573

[14] Metternicht G. Vegetation indices derived from high-resolution airbone videography for precision crop management. International Journal of Remote Sensing. 2003;24(14):2855-2877. DOI: 10.1080/01431160210163074

[15] Moskowitz C. The Mars Resonnaissance Orbiter found evidence that flowing water causes suspicious

dark streaks on the Red Planet. Scientific American [Internet]. 2015. Available from: https://www.scientificamerican.com/article/water-flows-on-mars-today-nasa-announces/ [Accessed: 2021-02-15]

[16] Wilson JT, Eke VR, Massey RJ, Elphic RC, Feldman WC, Maurice S, Teodoro LFA. Equatorial locations of water on Mars: improved resolutions maps based on Mars Odyssey Neutron Spectrometer data. Icarus. 2018;299: 148-160. DOI: 10.1016/j.icarus.2017.07.028

[17] Mattar C, Sobrino JA, Wigneron JP, Jiménez-Muñoz JC, Kerr Y. Estimación de la humedad del suelo a partir de índices de vegetación y microondas pasivas. Revista de Teledetección. 2011; 36:62-72. DOI: http://www.aet.org.es/?q=revista36-8

[18] Pinnington E, Amezcua J, Cooper E, Dadson S, Ellis R, Peng J, Robinson E, Morrison R, Osborne S, Quaife T. Improving soil moisture prediction of a high-resolution land surface model by parameterizing pedotransfer functions through assimilation of SMAP satellite data. Hydrology and Earth System Science. 2021;25:1617-1641. DOI: 10.5194/hess-25-1617-2021

[19] Cheruy F, Ducharne A, Hourdin F, Musat I, Vignon E, Gastineau G, Bastrikov V, Vuichard N, Diallo B, Dufresne JL, Ghattas J, Grandpeix JY, Idelkadi A, Mellul L, Maignan F, Ménégoz M, Ottlé C, Peylin P, Servonnat J, Wang F, Zhao Y. Improved near-surface continental climate in IPSL-CM6A-LR by combined evolutions of atmospheric and land surface physics. Journal of Advances in Modelling Earth Systems. 2020;12(10):1-33. DOI: 10.1029/2019MS002005

[20] Chen JM, Liu J. Evolution of evapotranspiration models using thermal and shortwave remote sensing data. Remote Sensing of Environment. 2020;237:1-20. DOI: 10.1016/j.rse.2019.111594

[21] NASA. The mars Exploration Rovers: Spirit and Opportunity. [Internet]. 2013. Available from: https://mars.nasa.gov/files/resources/MER10-YearAnniversaryLithograph.pdf [Accessed: 2021-02-16]

[22] NASA/JPL/Cornell. Eagle Crater (Mars Exploration Rover Opportunity). [Internet]. 2004. Available from: https://mars.nasa.gov/mer/gallery/press/opportunity/20040506a/02-SS-02-OpportunityLedge-B101R1_br.jpg [Accessed: 2021-02-18]

[23] Zotarelli L, Dukes MD, Morgan KT. Interpretation of soil moisture content to determine soil field capacity and avoid over-irrigating sandy soils using soil moisture sensors. EDIS. 2010;2:1-4. DOI: http://edis.ifas.ufl.edu/ae460

[24] Seybold HJ, Kite E, Kirchner JW. The role of surface water in the geometry of Mars' valley networks and its climatic implications. [Internet]. 2017. Available from: https://arxiv.org/abs/1709.09834 [Accessed: 2021-02-16]

[25] NASA/JPL/Cornell. Endurance Crater (Mars Exploration Rover Opportunity). [Internet]. 2004. Available from: https://photojournal.jpl.nasa.gov/catalog/PIA06727 [Accessed: 2021-02-18]

[26] Arvidson RE, Ashley JW, Bell III JF, Chojnacki M, Cohen J, Economou TE, Farrand WH, Fergason R, Fleischer I, Geissler P, Gellert R, Golombek MP, Grotzinger JP, Guinness EA, Haberle RM, Herkenhoff KE, Herman JA, Iagnemma KD, Jolliff BL, Johnson JR, Klingelhöfer G, Knoll AH, Knudson AT, Li R, McLennan SM, Mittlefehldt DW, Morris RV, Parker TJ, Rice MS, Schröder C, Soderblom LA, Squyres SW, Sullivan RJ, Wolff MJ. Opportunity Mars Rover mission: overview and selected results from

Purgatory ripple to traverses Endeavour crater. Journal of Geophysical Research. 2011;116:1-33. DOI: 10.1029/2010JE003746

[27] NASA/JPL/Cornell. Wopmay rock in Endurance Crater (Mars Exploration Rover Opportunity). [Internet]. 2004. Available from: https://photojournal.jpl.nasa.gov/catalog/PIA06920 [Accessed: 2021-02-18]

[28] CSIC-INTA. Rover Environmental Monitoring Station. [Internet]. 2009. Available from: http://cab.inta-csic.es/rems/es/atmosfera-de-marte/ [Accessed:2021-01-06]

[29] Dall'Osto L, Cazzaniga S, North H, Marion-Poll A, Bassi R. The Arabidopsis aba4-1 mutant reveals a specific function for neoxanthin in protection against photooxidative stress. The Plant Cell. 2007;19:1048-1064. DOI: 10.1105/tpc.106.049114

[30] García S, Pérez RM. Aspectos analíticos sobre la determinación de compuestos carotenoids en microalgas mediante cromatografía de líquidos con detector de diodos. [Internet]. 2012. Available from: https://www.osti.gov/etdeweb/servlets/purl/21542049 [Accessed: 2021-02-07]

[31] Ramírez-Juidías E, Yanes-Figueroa J. Estudio medioambiental del municipio de almadén mediante teledetección. Interciencia. 2017;42(3):157-162. DOI: https://www.interciencia.net/wp-content/uploads/2017/08/157-162-5834-RAMIREZ-42_3.pdf